Electronic Supplementary Material (ESI) for Nanoscale Advances.

Supporting information:

Mechanisms of sodiation in anatase TiO_2 in terms of equilibrium thermodynamics and kinetics

Zhongqiu Tong, Tianxing Kang, Jianming Wu, Rui Yang, Yan Wu, Ruqian Lian, Hui Wang, Yongbing Tang, Chun-Sing Lee

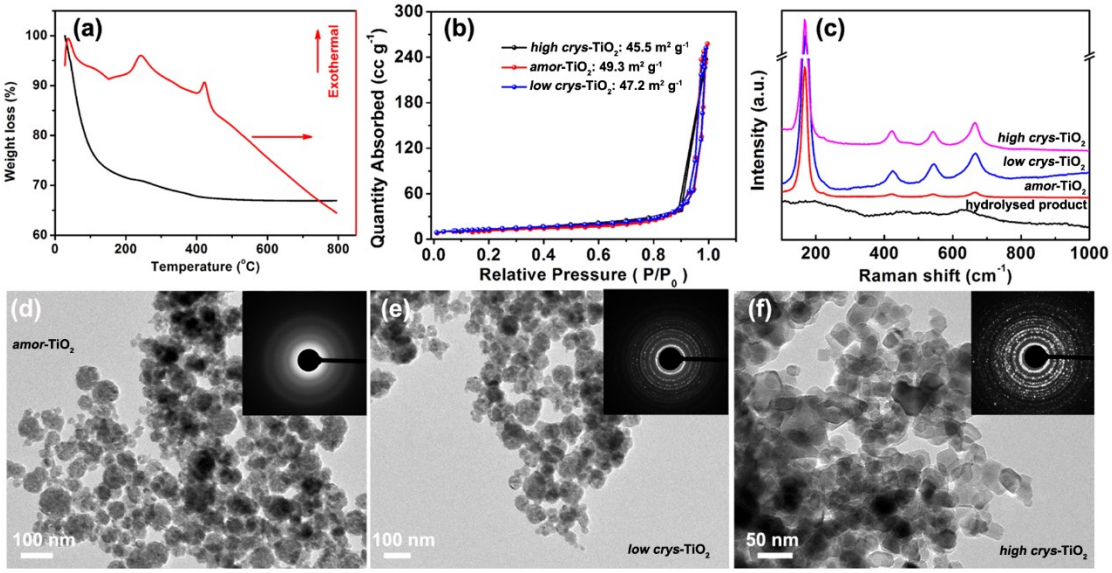

Fig. S1. (a) TGA-DSC curves of the hydrolyzed titania nanoparticles. Nitrogen adsorption/desorption isotherms (b) and Raman spectra (c) of the *amor*-TiO_2, the *low crys*-TiO_2 and the *high crys*-TiO_2 materials. TEM images and SAED patterns of the *amor*-TiO_2 (d), the *low crys*-TiO_2 (e) and the *high crys*-TiO_2 (f) materials.

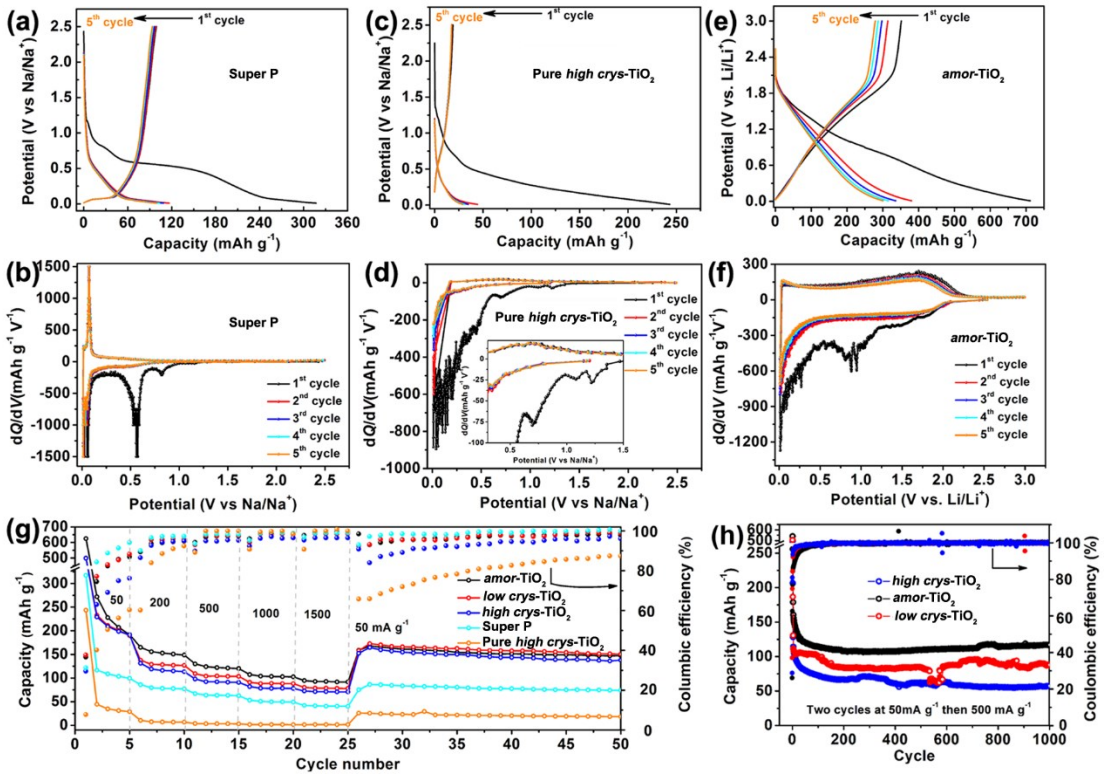

Fig. S2. Discharge/charge profiles and corresponding differential (*dQ*/*dV*) curves of the super P Na-ion (a,b), the pure *high crys*-TiO_2 (c,d) and the *amor*-TiO_2 Li-ion electrodes (e,f) at 50 mA g^{-1}. Rate performance (g) and cycling performance (h) of the *amor*-TiO_2, the *low crys*-TiO_2 and the *high crys*-TiO_2 anodes.

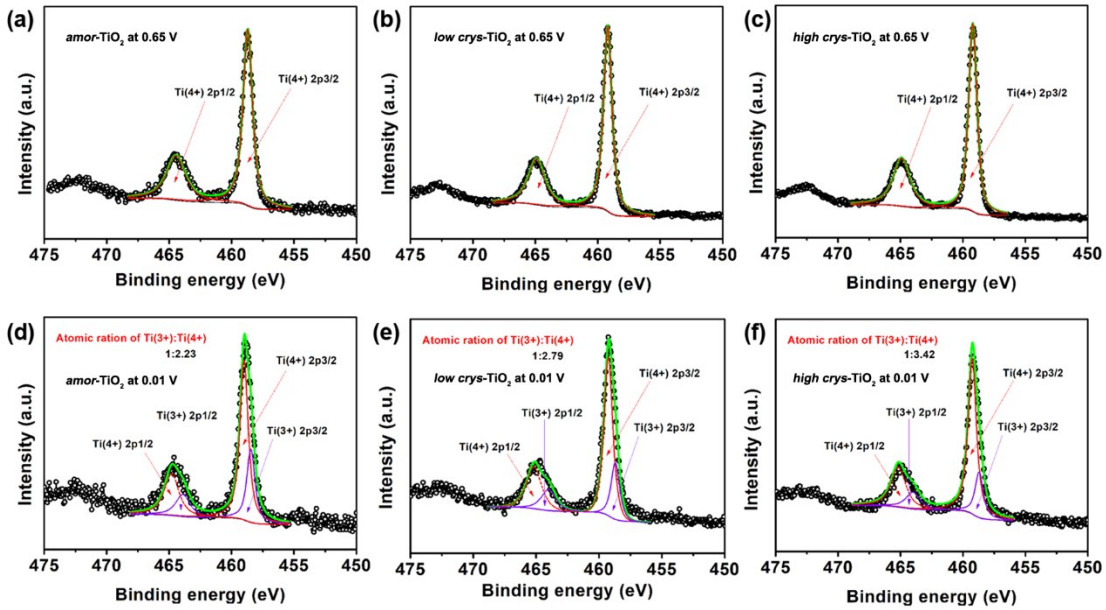

Fig. S3. XPS spectra of Ti 2p in of the *amor*-TiO_2 (a), the *low crys*-TiO_2 (b) and the *high crys*-TiO_2 (c) electrodes at 0.65 V under 1st galvanostatic discharge at 50 mA g^{-1}. XPS spectra of Ti 2p in of the *amor*-TiO_2 (d), the *low crys*-TiO_2 (e) and the *high crys*-TiO_2 (f) electrodes at 0.01 V under 1st galvanostatic discharge at 50 mA g^{-1}.

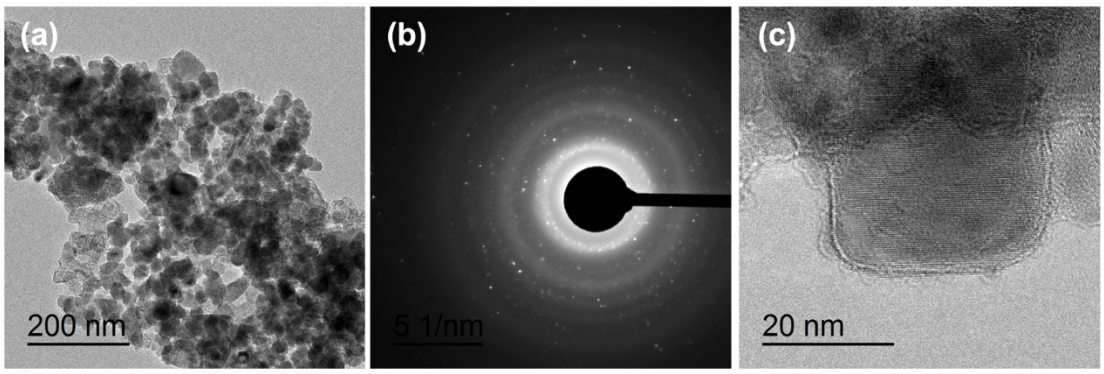

Fig. S4. TEM (a) and SAED pattern (b) of the *high crys*-TiO_2 after being fully discharge at 50 mA g^{-1} after 1st galvanostatic discharge under 50 mA g^{-1}. (c) HRTEM images of an unreacted anatase TiO_2 nanoparticle taken from the *high crys*-TiO_2 electrode after 1st galvanostatic discharge under 50 mA g^{-1}.

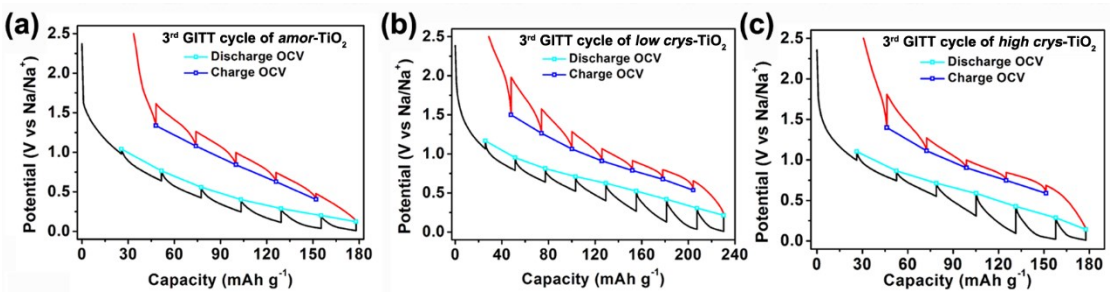

Fig. S5. 3rd GITT sodium-ion uptake/release profiles of the *amor*-TiO_2 (a), the *low crys*-TiO_2 (b) and the *high crys*-TiO_2 (c) electrodes.

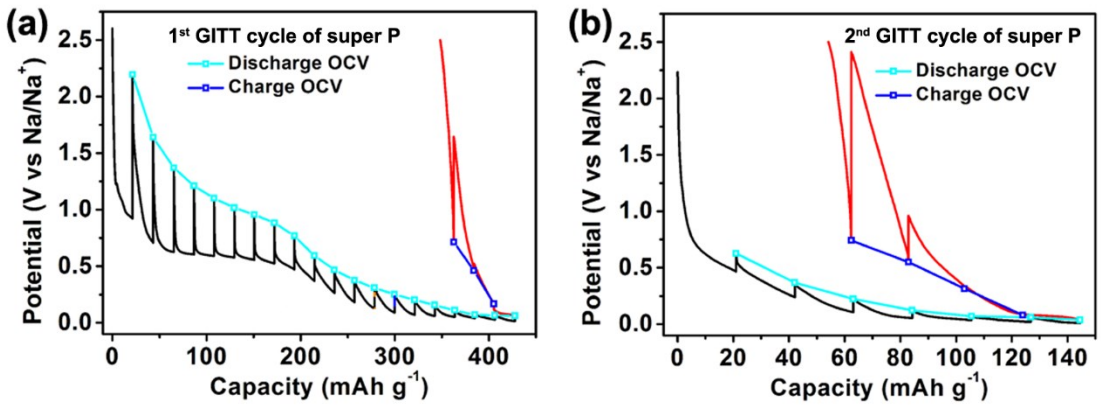

Fig. S6. 1st (a) and 2nd (b) GITT sodium-ion uptake/release profiles of the super P electrodes.

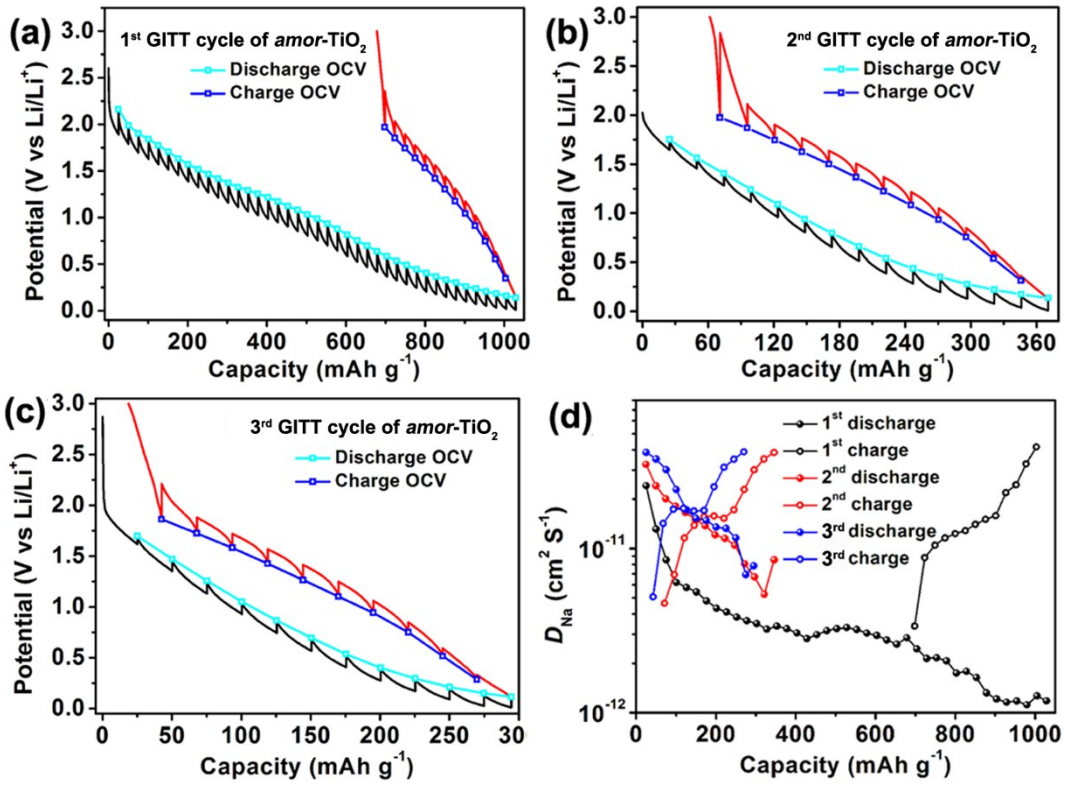

Fig. S7. 1st (a), 2nd (b) and 3rd (c) GITT lithiation/de-lithiation of the *amor*-TiO_2 electrode. (d) D_{Li} calculated from the GITT lithiation/de-lithiation of the *amor*-TiO_2 electrode of the 1st, the 2nd and the 3rd GITT cycles.

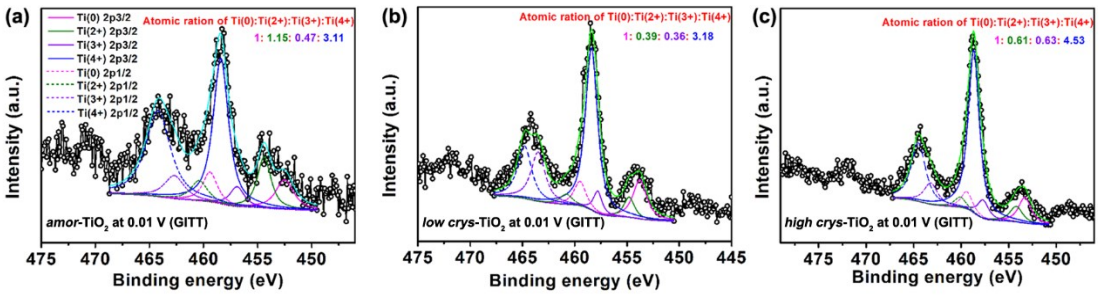

Fig. S8. XPS spectra of Ti 2p in of the *amor*-TiO_2 (a), the *low crys*-TiO_2 (b) and the *high crys*-TiO_2 (c) electrodes at 0.01 V under the 1st GITT discharge at 25 mA g^{-1} with 24 h relaxation.

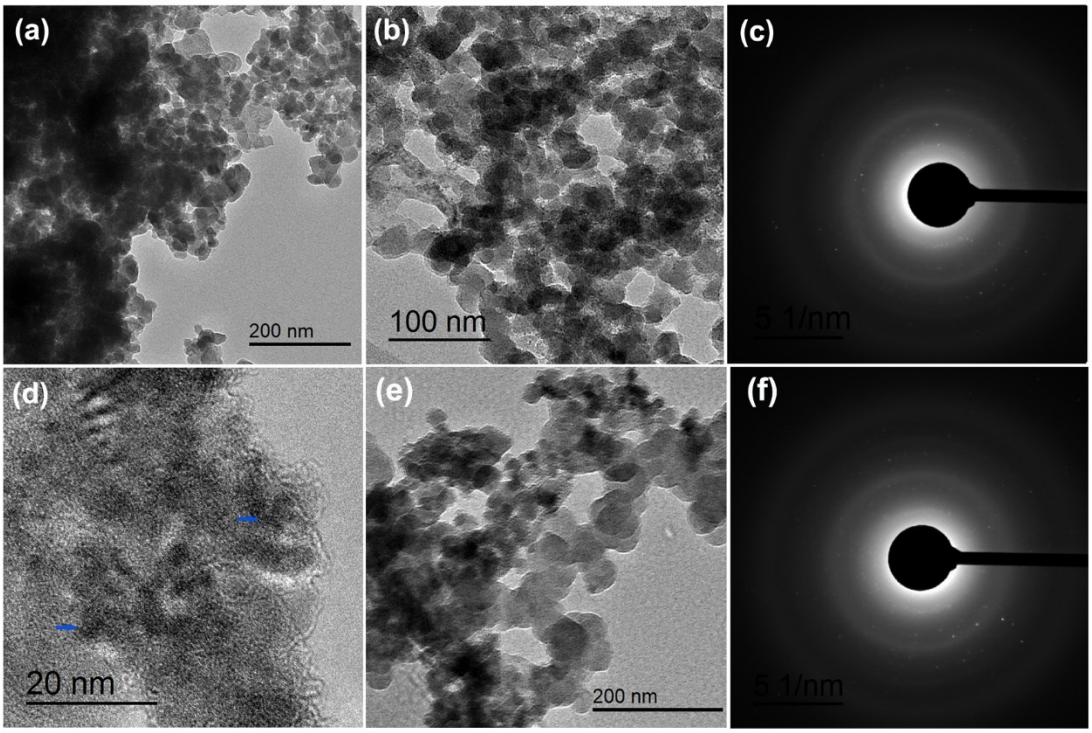

Fig. S9. TEM images (a,b), SAED pattern (c) and HRTEM image (d) of the *high crys*-TiO_2 after the 1st GITT sodiation. TEM image (e) and SAED pattern (f) of the *high crys*-TiO_2 after the 1st GITT sodiation/de-sodiation.

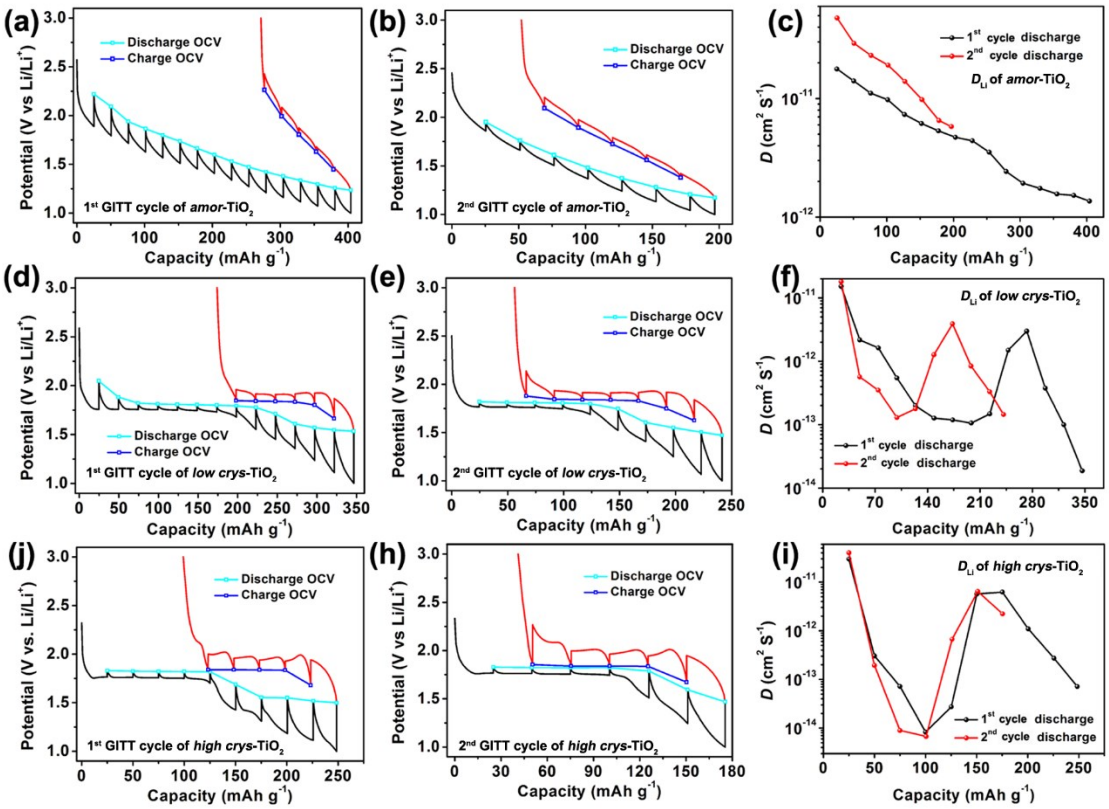

Fig. S10. GITT profiles of the *amor*-TiO_2 Li-ion anode in the 1st (a) and 2nd (b) cycle over the potential region from 1 to 3 V. (c) D_{Li} values calculated from the 1st and 2nd GITT discharge profiles of the *amor*-TiO_2 Li-ion anode. GITT profiles of the *low crys*-TiO_2 Li-ion anode in the 1st (d) and the 2nd (e) cycle over the potential region from 1 to 3 V. (f) D_{Li} values calculated from the 1st and the 2nd GITT discharge profiles of the *low crys*-TiO_2 Li-ion anode. GITT profiles of the *high crys*-TiO_2 Li-ion anode in the 1st (j) and the 2nd (h) cycle over the potential region from 1 to 3 V. (i) D_{Li} values calculated from the 1st and the 2nd GITT discharge profiles of the *high crys*-TiO_2 Li-ion anode.

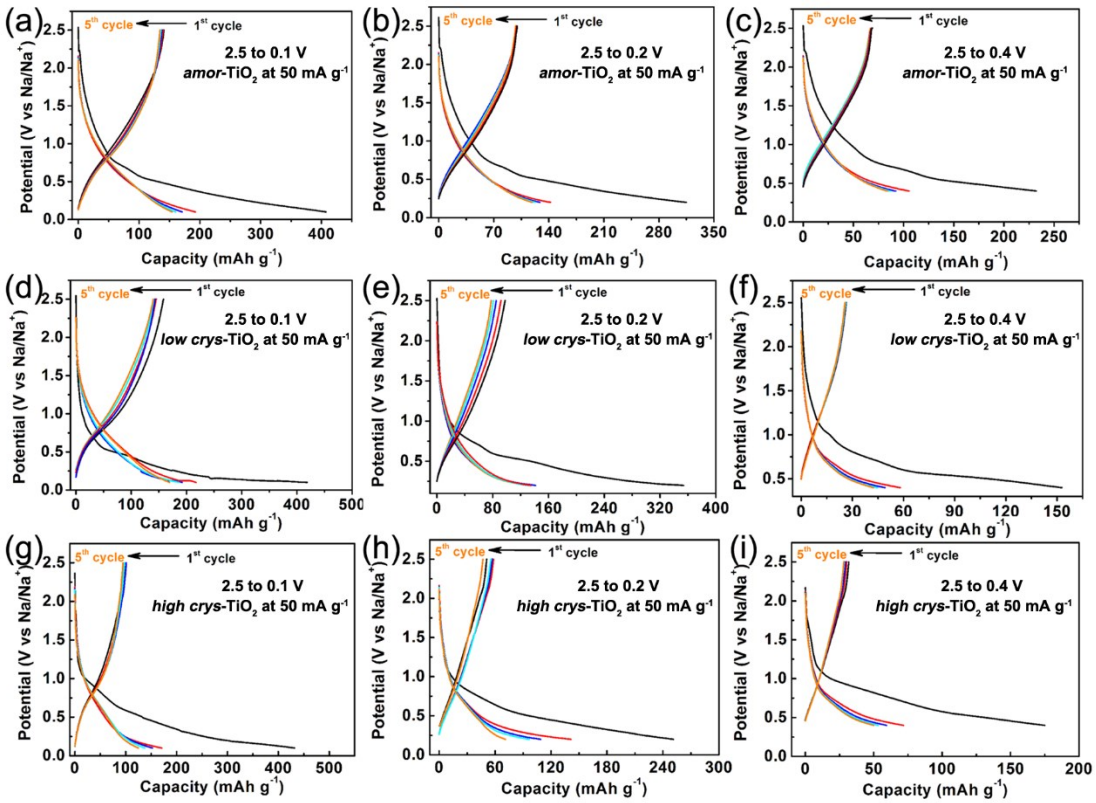

Fig. S11. Discharge/charge profiles of the TiO_2 Na-ion electrodes over different cut-off potentials at 50 mA g^{-1}. (a,b,c) The *amor*-TiO_2 electrodes. (d,e,f) The *low crys*-TiO_2 electrodes. (g,h,i) The *high crys*-TiO_2 electrodes.

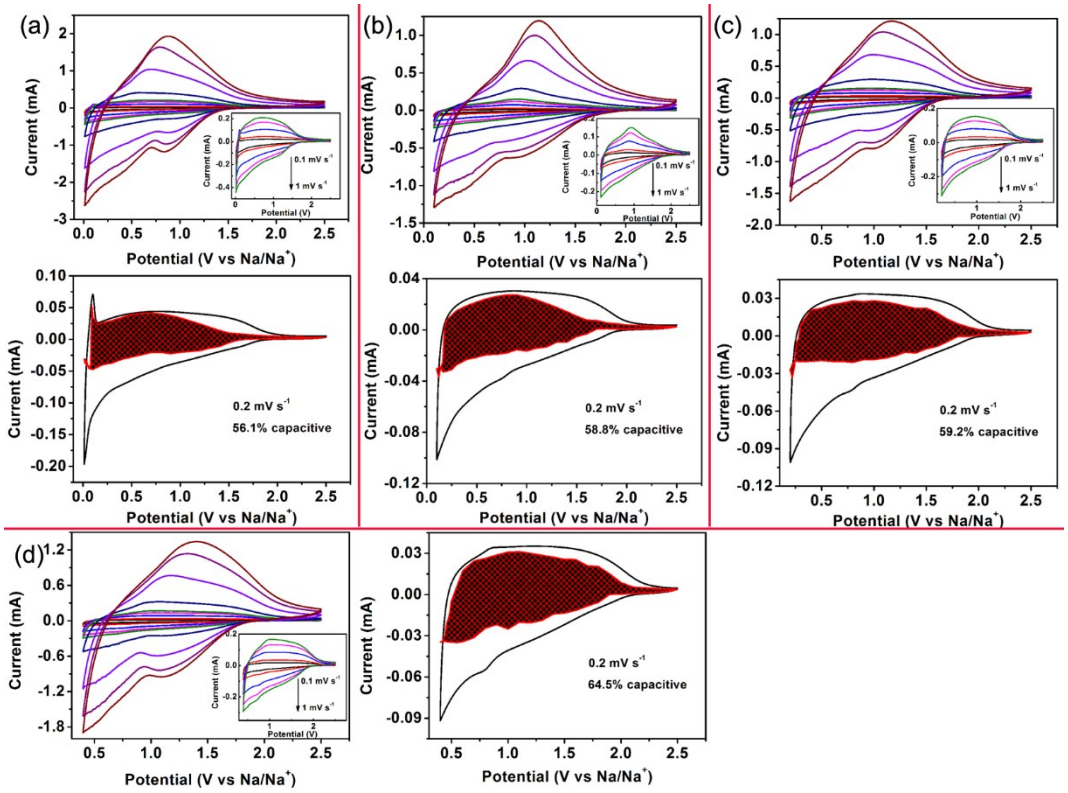

Fig. S12. Calculation of the capacitive contribution ratio over different cut-off potentials for the *amor*-TiO_2 electrodes. (a) Potential window from 0.01 to 2.5 V. (b) Potential window from 0.1 to 2.5 V. (c) Potential window from 0.2 to 2.5 V. (d) Potential window from 0.4 to 2.5 V.

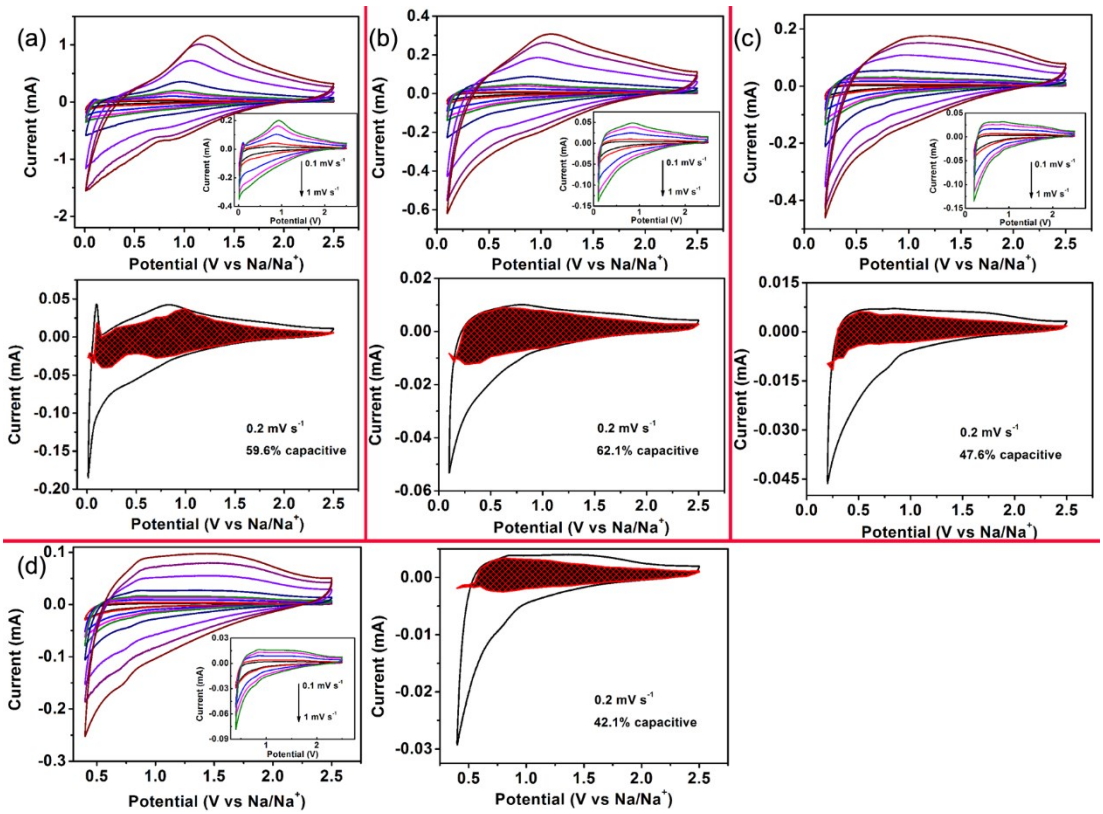

Fig. S13. Calculation of the capacitive contribution ratio over different cut-off potentials for the *low crys*-TiO_2 electrodes. (a) Potential window from 0.01 to 2.5 V. (b) Potential window from 0.1 to 2.5 V. (c) Potential window from 0.2 to 2.5 V. (d) Potential window from 0.4 to 2.5 V.

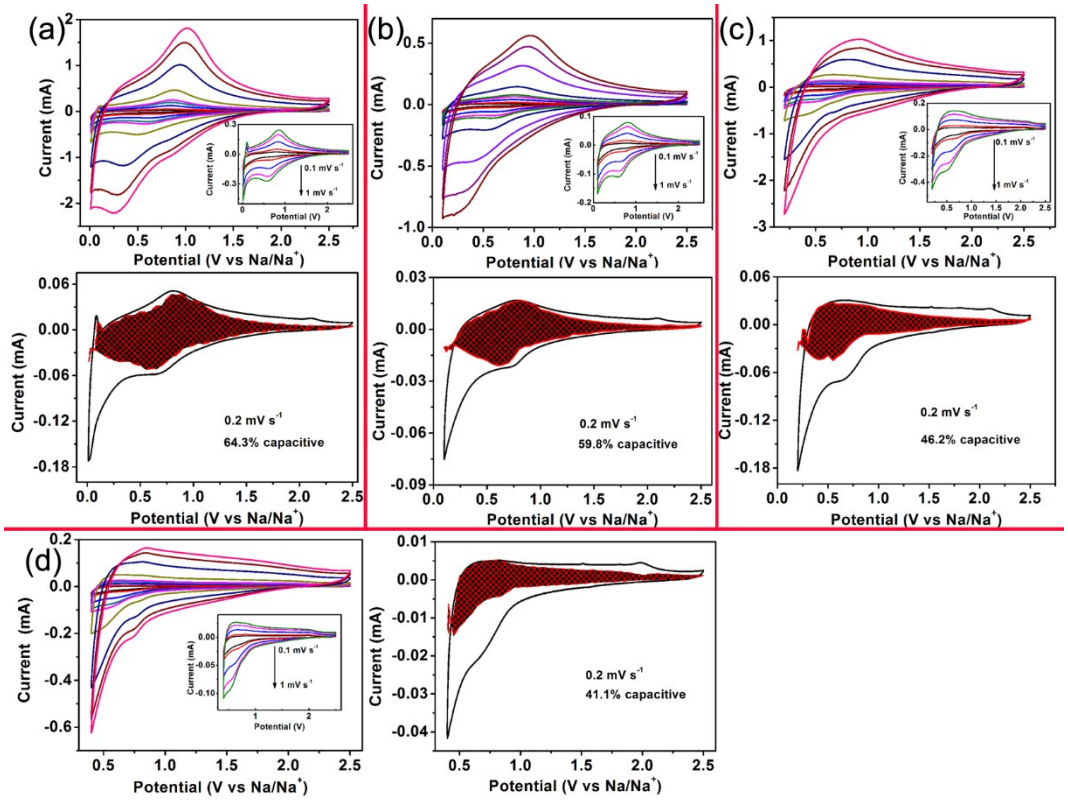

Fig. S14. Calculation of the capacitive contribution ratio under different cut-off potentials for the *high crys*-TiO_2 electrodes. (a) Potential window from 0.01 to 2.5 V. (b) Potential window from 0.1 to 2.5 V. (c) Potential window from 0.2 to 2.5 V. (d) Potential window from 0.4 to 2.5 V.

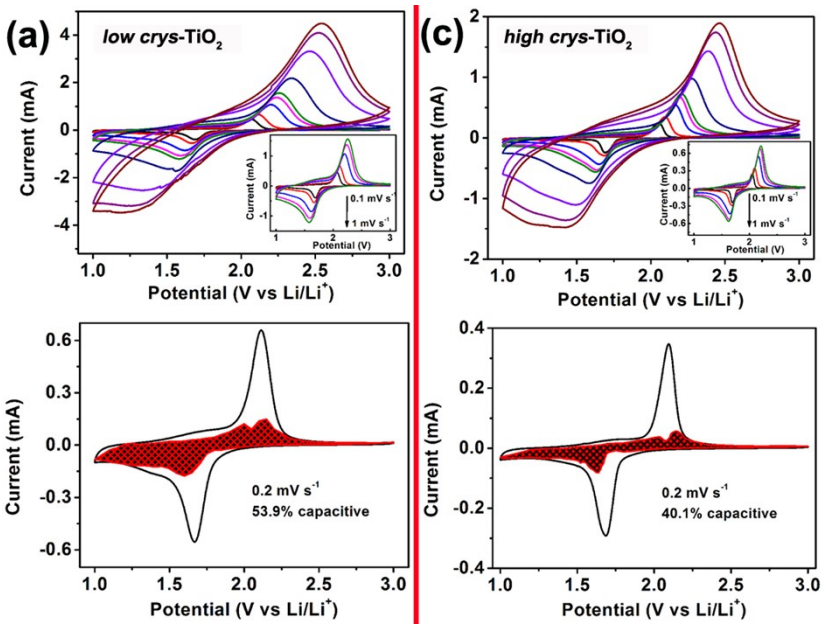

Fig. S15. Calculation of the capacitive contribution ratio for the *low crys*-TiO_2 (a) and the *high crys*-TiO_2 Li-ion electrodes over potential window from 1 to 3 V.

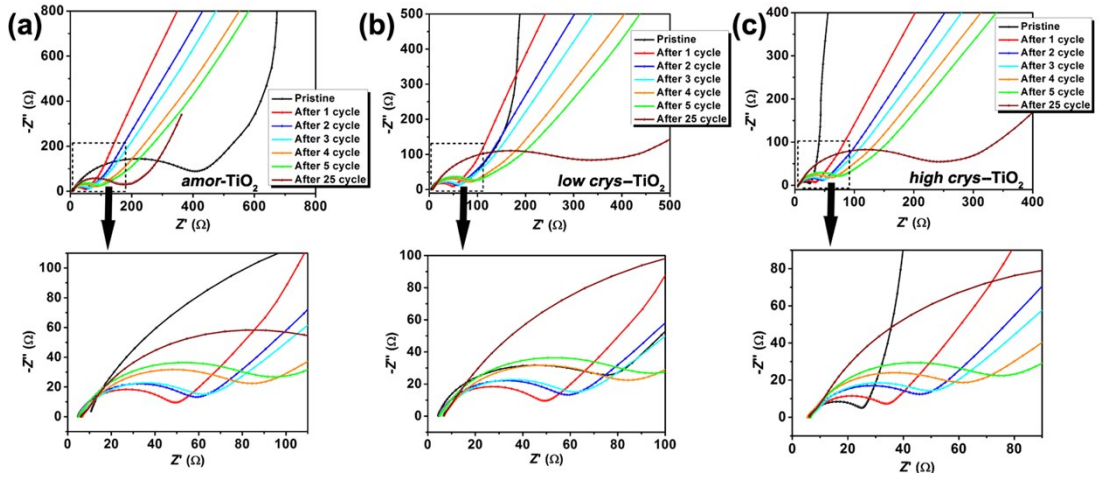

Fig. S16. EIS of the *amor*-TiO_2 (a), the *low crys*-TiO_2 (b) and the *high crys*-TiO_2 (c) Na-ion half cells after different cycles at 50 mA g^{-1} over the potential window of 0.01 to 2.5 V.

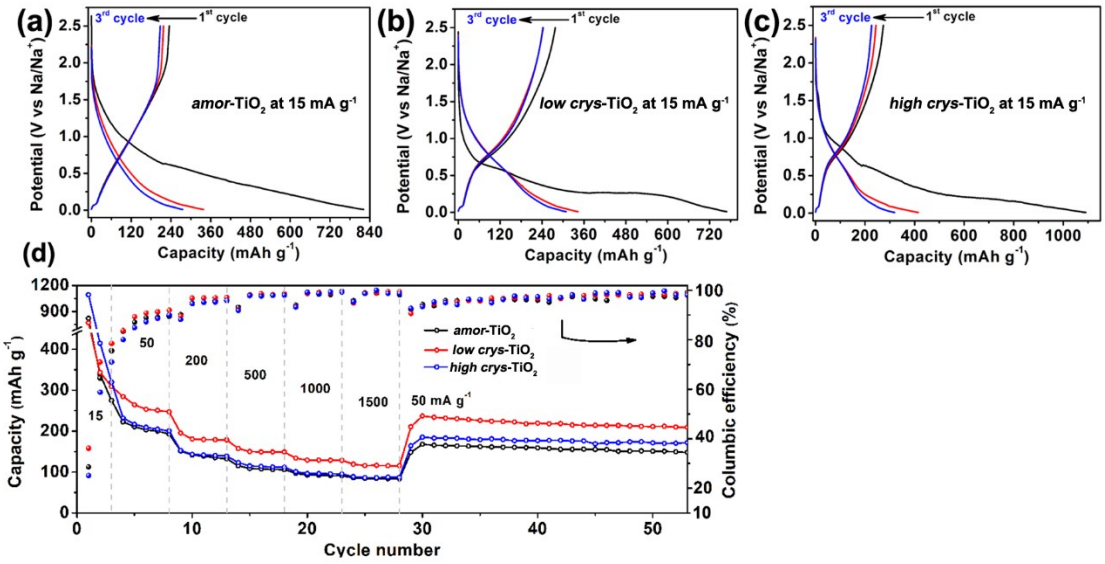

Fig. S17. Discharge/charge profiles of the *amor*-TiO_2 (a), the *low crys*-TiO_2 (b) and the *high crys*-TiO_2 Na-ion (c) electrodes at 15 mA g^{-1}. (d) Rate performance of the *amor*-TiO_2, the *low crys*-TiO_2 and the *high crys*-TiO_2 electrodes with initially applied current density of 15 mA g^{-1}.

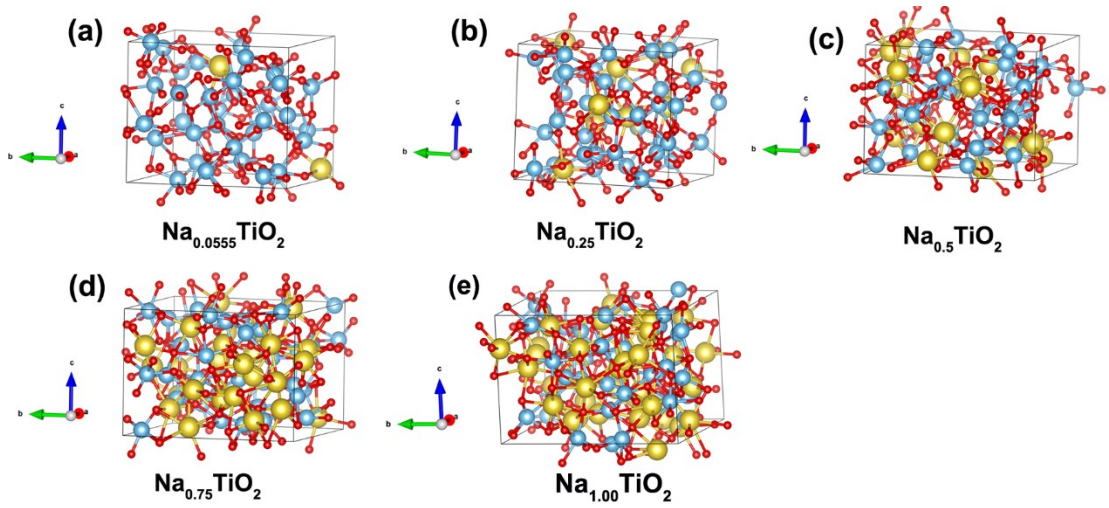

Fig. S18. Structural models of the amorphous TiO_2-derived $Na_{0.0555}TiO_2$ (a), $Na_{0.25}TiO_2$ (b), $Na_{0.5}TiO_2$ (c), $Na_{0.25}TiO_2$ (d), and $NaTiO_2$ (e).

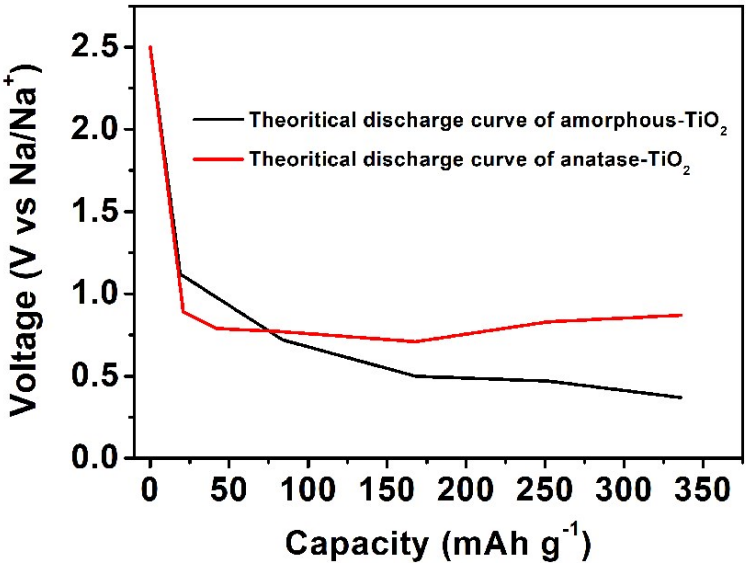

Fig. S19. Theoretical discharge curves of amorphous and anatase TiO_2 materials up to corresponding $NaTiO_2$.

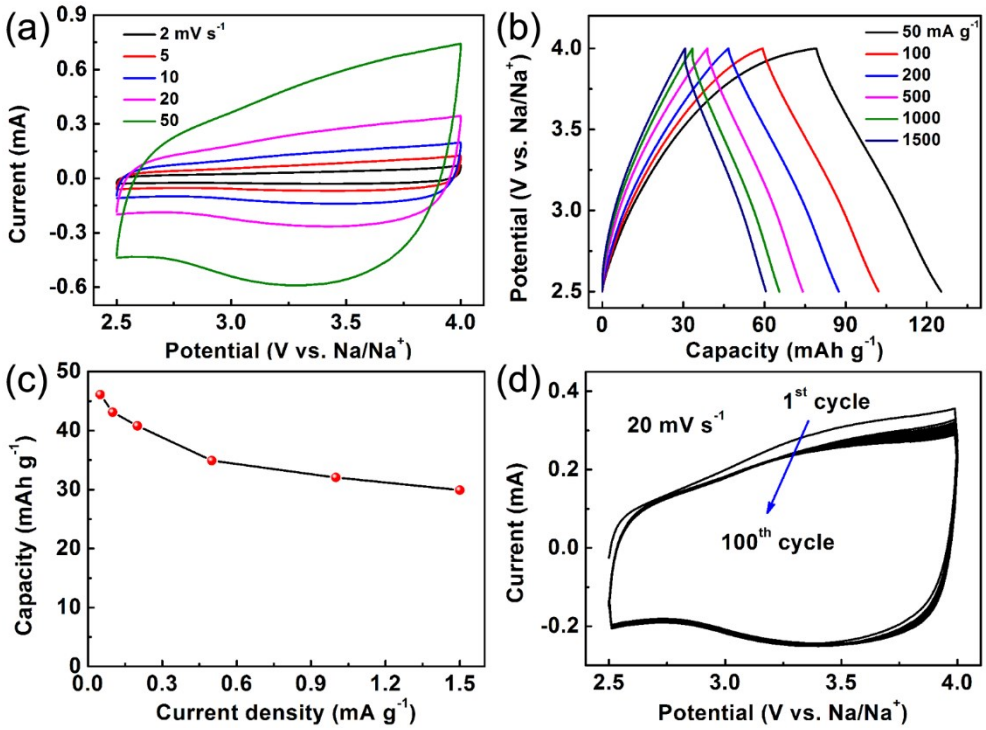

Fig. S20. Electrochemical performance of AC Na-ion cathodes. (a) CV curves of an AC Na-ion cathode under different scan rates. (b) Charge/discharge profiles of an AC Na-ion cathode under different current densities. (c) Rate performance of an AC Na-ion cathode. (d) CV stability of an AC Na-ion cathode at 20 mV s^{-1} for 100 cycles.

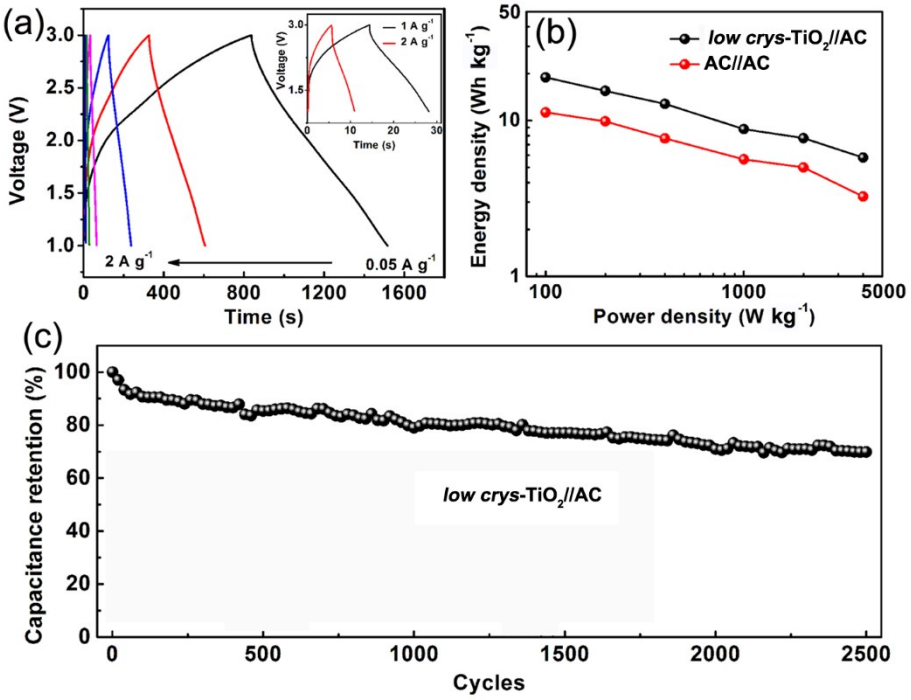

Fig. S21. Electrochemical performance of the *low crys*-TiO_2//AC hybrid capacitor. (a) Charge/discharge profiles of a hybrid capacitor under different current densities. (b) Ragon plots of the *low crys*-TiO_2//AC and the AC//AC capacitors. (c) Cycling performance of the *low crys*-TiO_2//AC hybrid capacitor at 200 mA g^{-1}.

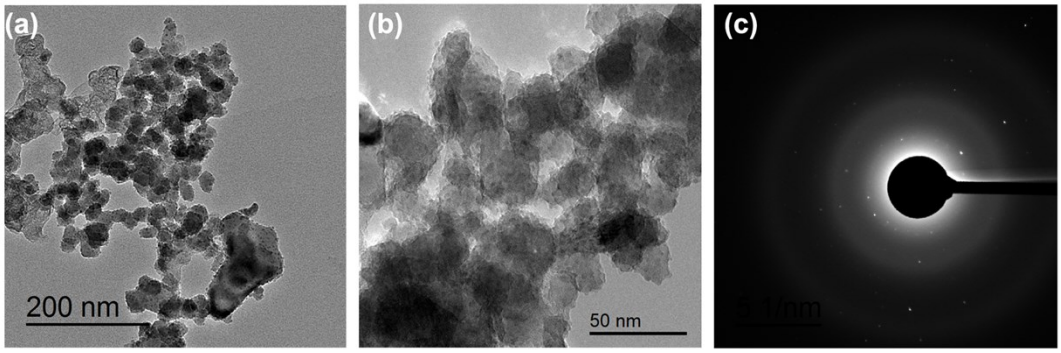

Fig. S22. (a)(b) TEM images and SAED pattern of *low crys*-TiO_2 samples of *low crys*-TiO_2//AC hybrid capacitor after 2500 cycles at 200 mA g^{-1}.